Supplemental Information

Figure S1, related to Figure 1. Regional differences in oral epithelial clonal growth despite similar proliferation rates.

Figure S2, related to Figure 3. Label retaining cells in palate are rare, slow-cycling, and not sensory neurons.

Figure S3, related to Figure 4. Establishment and characterization of 7d puncture wounding model.

Figure S4, related to Figure 5. Establishment and characterization of soft diet “stress-mitigating” assay.

Figure S5, related to Figure 6. RNAseq reveals Lrig1 is enriched in quiescent OESCs of the JZ.

Figure S6, related to Figure 7**.** Lrig1 labels JZ LRCs and maintains quiescence.

Supplemental File 1, related to Figure 5. RNAseq and lineage tracing reveals that Lrig1 marks IDCs.

Figure S1, related to Figure 1

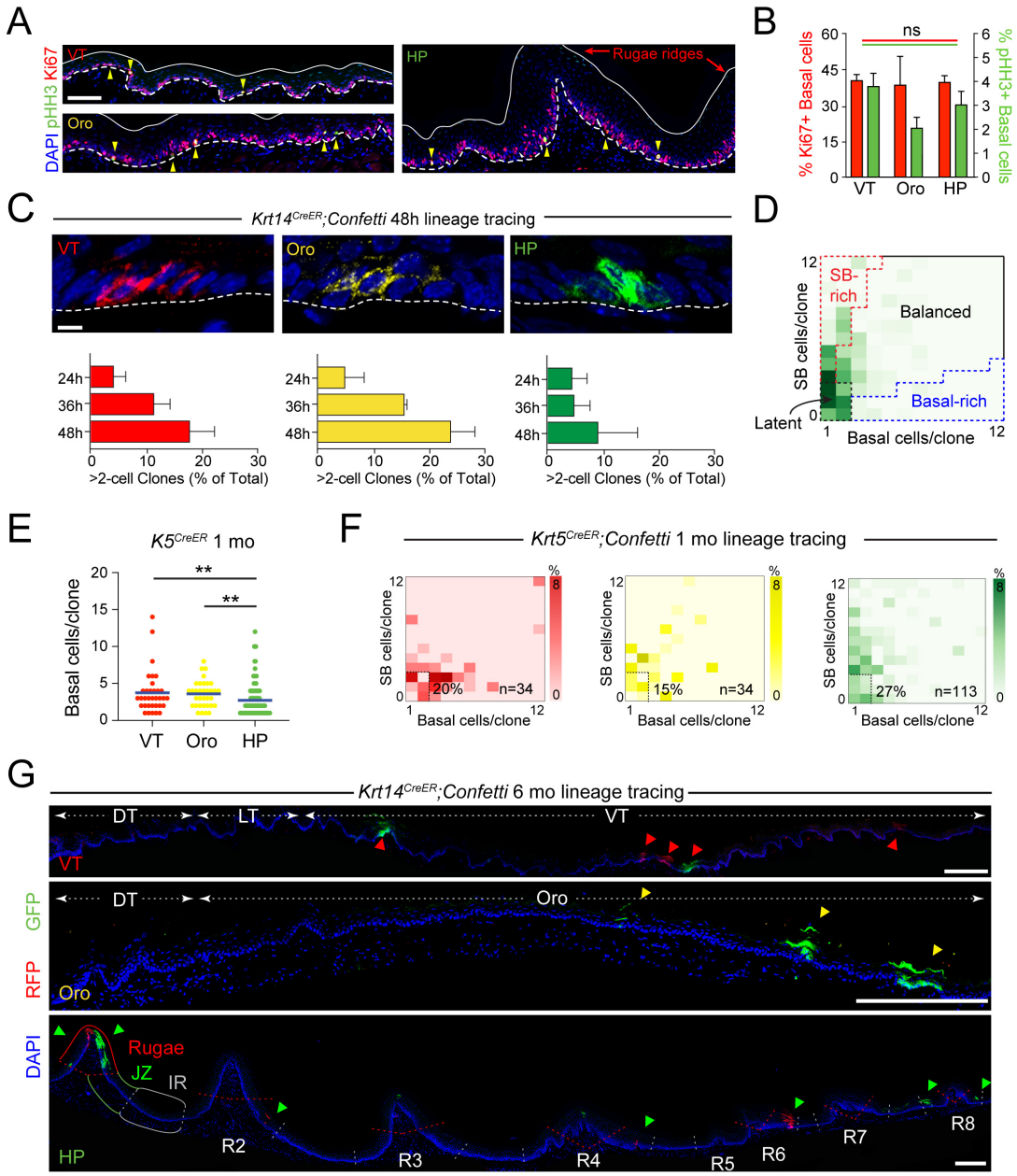

Figure S1, related to Figure 1 | Regional differences in oral epithelial clonal growth despite similar proliferation rates

(A) Sagittal sections of ventral tongue (VT), oropharynx (Oro) and hard palate (HP) labeled with markers of mitosis (pHH3, green, and yellow arrowheads) and active cycling (Ki67, red), quantified in (B). Dashed white lines indicate position of basement membrane while solid white lines in represent position of epithelial surface. (C) Representative images of >2 cell clones at 48h timepoint in indicated regions, with quantification of >2-cell clone frequency at 24, 36, and 48h by region. (D) Example of a clonal density array (CDA), which allows visualization of total clonal distribution by plotting the frequency of clones by basal (x-axis) and suprabasal (SB, y-axis) cell/clone. Darker colors (higher color value) indicate higher frequencies of specific clone types. Clone types are categorized as follows: 1) latent ($\leq$2 basal cells and $\leq$2 SB cells/clone); 2) basal-rich (B:SB ratio $\geq$3), 3) suprabasal-rich (SB:B ratio $\geq$3), and 4) balanced (all others). (E,F) Lineage tracing using *Krt5*^{CreER}, another basal OE driver (compare to *Krt14*^{CreER} in Figure 1G,H). (G) Tilescans of clones in ventral tongue, oropharynx and hard palate regions after long-term (6 mo) lineage tracing. Note that many persistent clones are found in the HP junctional zone (JZ), located between the rugae peaks (R, demarcated by red dashed lines) and interrugae (IR, demarcated by white dashed lines). DT, dorsal tongue; LT, lateral tongue; arrowheads indicate position of clones. ns, not significant, *p<0.05, **p<0.01, ***p<0.0001, by Student's t-test in (B), Mann-Whitney test in (E). Error bars in (B,C) represent s.e.m. Scale bars: 50 μm (A), 10 μm (C), 250 μm (G).

Figure S2, related to Figure 3

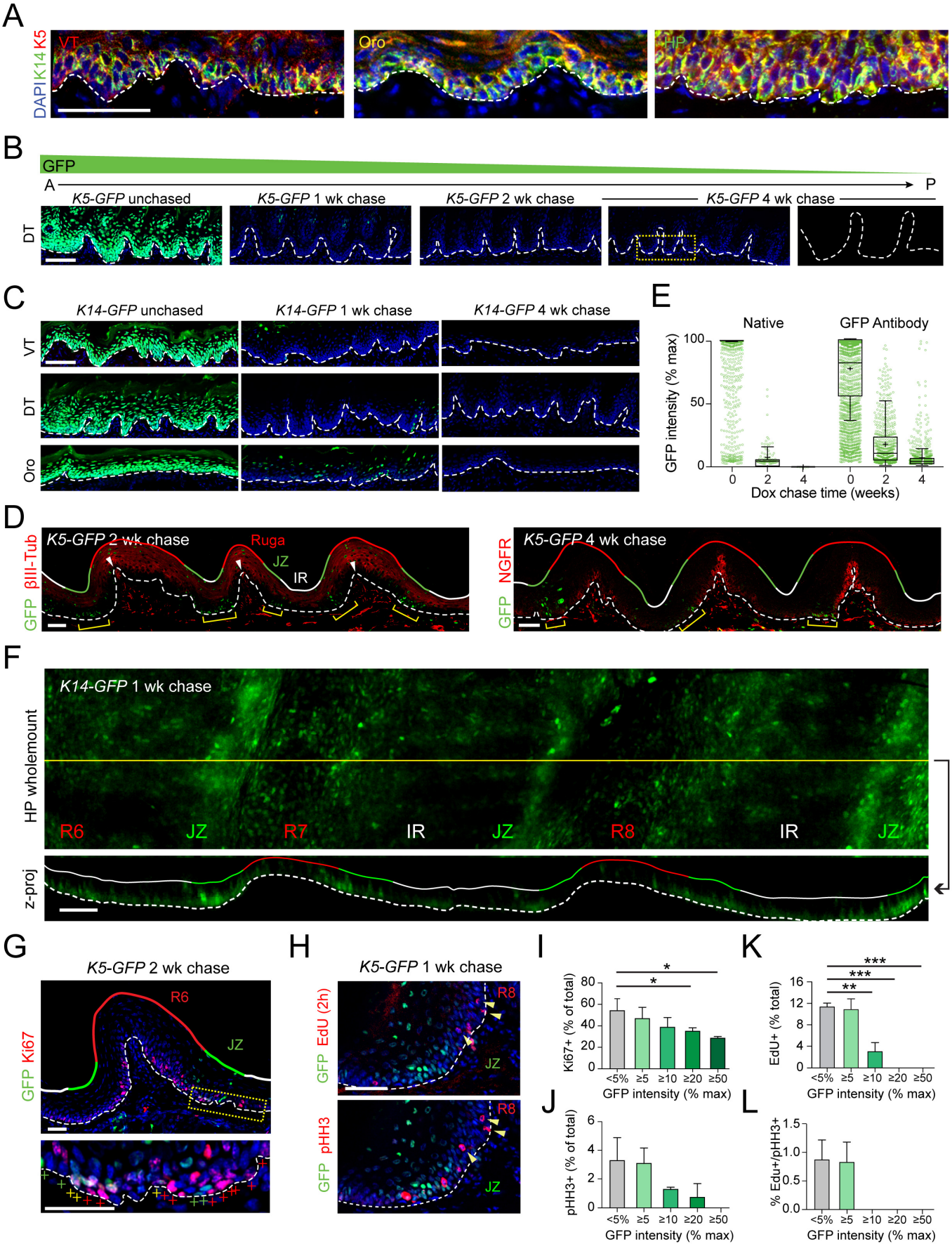

Figure S2, related to Figure 3 | Label retaining cells in palate are rare, slow-cycling, and not sensory neurons
(A) Expression of basal keratins K5 and K14 in ventral tongue (VT), oropharynx (Oro) and hard palate (HP). (B) Images of *K5-GFP* dorsal tongue (DT) chased for 0, 1, 2, or 4 wks; companion to Figure 3C; boxed area shown at high magnification at right. (C) Similar to (B), but with *K14-GFP* line. (D) Section of hard palate, showing localization of IDCs (green) relative to neuronal afferents (red), labeled with βIII-tubulin or p75/NGFR. Note innervation is restricted to ruga peaks while IDCs (yellow bracketed regions) are generally found on ruga slopes. (E) Quantification of GFP fluorescence intensity after fixation in fresh frozen sections without antibody amplification ("native") and with antibody amplification. With no antibody, IDCs are virtually absent in the hard palate by 4 wks post-chase (left). GFP antibody amplification demonstrates the best stratification of GFP intensities at 2 wks post-chase with a minority of IDCs ($\geq$20% max intensity) and a majority of FDCs (<5% max) (right). (F) Whole mount (top), and maximum z-projection at position of yellow line (bottom) of *K14-GFP* after 1 wk chase. LRCs are concentrated at JZs (green) on the rugae slopes. (G) R6 showing that LRCs (GFP, green) infrequently colabel with Ki67 (red). Boxed area shown at high magnification below; + signs indicate Ki67+ (red), GFP+ (green) and double-positive (yellow). (H) R8 junctional zone (JZ) labeled with a 2h pulse of EdU (top) and mitotic marker pHH3 (bottom). EdU/pHH3 double-positive cells (arrowheads) are invariably GFP-. (I-L) Quantification of Ki67+ (I), pHH3+ (J), EdU+ (K), and pHH3+/EdU+ frequencies (L), binned by GFP levels, mean ± s.e.m. Positivity for all markers decreases with increasing GFP expression. White arrows in point to highest innervated area. Solid red, green, and white lines in (D-F) represent rugae (R), junctional zone (JZ), and interrugae (IR) zones, respectively. White dotted lines in (A-C, E-G) represent the basement membrane. Box and whisker plots in (E) demonstrate 95% CI. *p<0.05, **p<0.01, ***p<0.0001, by Student's t-test in (H,J). Scale bars: 50 μm except 100 μm in (F).

Figure S3, related to Figure 4

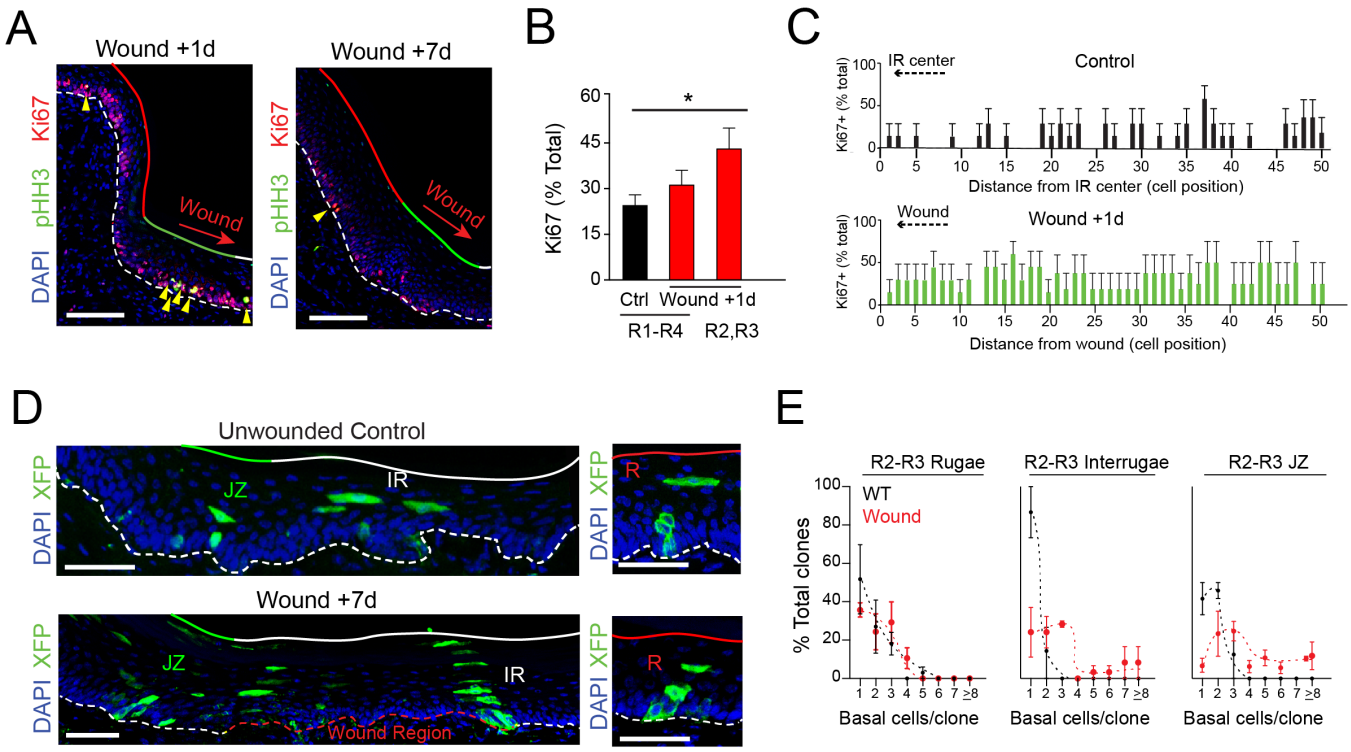

Figure S3, related to Figure 4 | Establishment and characterization of 7d puncture wounding model.
(A) Section of peri-wound area of R2 1d (left) and 7d (right) after wounding. Cycling (Ki67+, red) and mitotic (pHH3+, green, yellow arrowheads) are upregulated in the JZ (green solid line) near the wound 1 day after wounding; however, this activity is abrogated after healing by 7 days. Red arrows indicate direction of wound margin. (B) Proliferation, as assessed by Ki67 positivity in unwounded (black bar), versus 1d post-wound (red) tissue. Note peri-wound region (between R2 posterior slope and R3 anterior slope) shows highest increase in proliferation. (C) Cycling cell (Ki67+) frequency mapped by cellular distance from the wound site (1→50 cell positions anterior and posterior to wound site). In the 1d post-wound proximal space, cycling activity is upregulated along the entire region with the largest differences seen in the first 20 cells near the wound margin. (D) Lineage tracing using *K14^{CreER}; LSL-confetti* mice, treated with tamoxifen 1d before wounding. Clones were assessed 7d following wounding or in sham controls. Note migration of JZ clones into wound region. (E) Quantification of clone distribution by size in the unwounded (black) and wounded (red) R2/R3 region; plots are based on the same raw data as shown in Figure 4I. Bars in (B,C,E) represent s.e.m. *p<0.05, by Student's t-test. Scale bars: 100 μm (A), 50 μm (D).

Figure S4, related to Figure 5

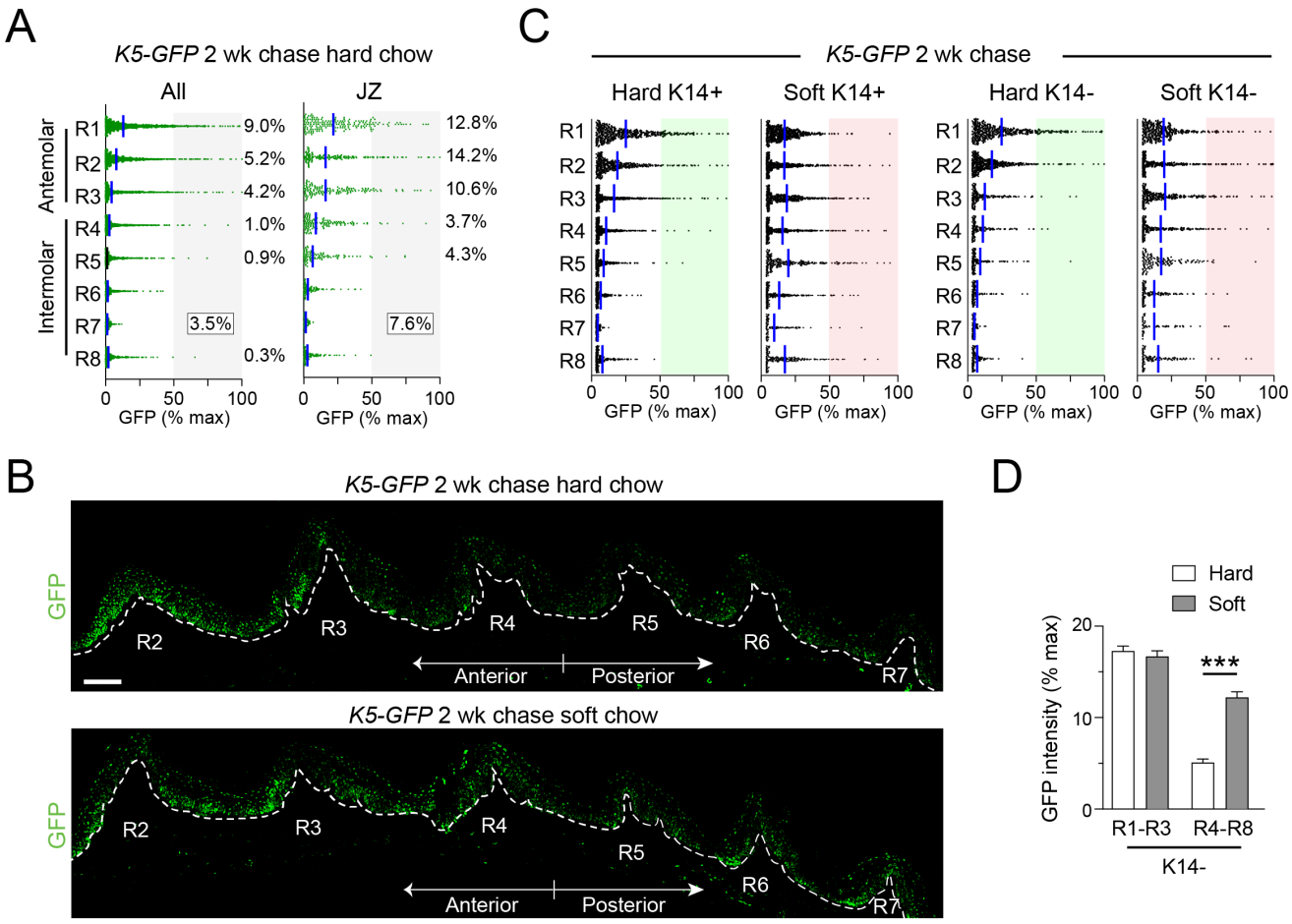

Figure S4, related to Figure 5 | Establishment and characterization of soft diet "stress-mitigating" assay.
(A) GFP intensity (% max) by ruga for *K5-GFP* mice following a 2 wk chase. On standard pelleted chow ("hard chow") there is an anteroposterior gradient of GFP label retention in whole rugae (All) and also in the junctional zone (JZ), where the highest label retention occurs anterior (antemolar rugae R1-R3) to the molars. Gray shaded areas indicate cells with GFP intensities >50% max ($GFP^{HI>50}$), corresponding to cells that divided one or fewer times. At right, the percentages of $GFP^{HI>50}$ cells within each ruga; in textbox, the percentage of $GFP^{HI>50}$ cells across the whole palate. (B) Confocal tilescan of R2-R7 region of HP, showing LRCs following a 2 wk chase on hard (top) or soft (bottom) chow. (C) Quantification of GFP intensity in each ruga in *K5-GFP* mice chased for 2 wks on hard or soft diet, separated by basal (K14+) and SB (K14-) populations. Both K14+ and K14- populations show higher label-retention in intermolar rugae in the soft diet condition. (D) Bar graph of data from (C) pooled into antemolar (R1-R3) and intermolar (R4-R8) groups. The observed increase in GFP intensity in the intermolar SB population is consistent with slower tissue turnover; this figure is the companion to Fig 5H, which shows data from basal cells. Blue bars in (A,C) represent the mean; error bars in (D) represent s.e.m. ***p<0.0001, by Student's t-test. Scale bar: 100 μm.

Figure S5, related to Figure 6

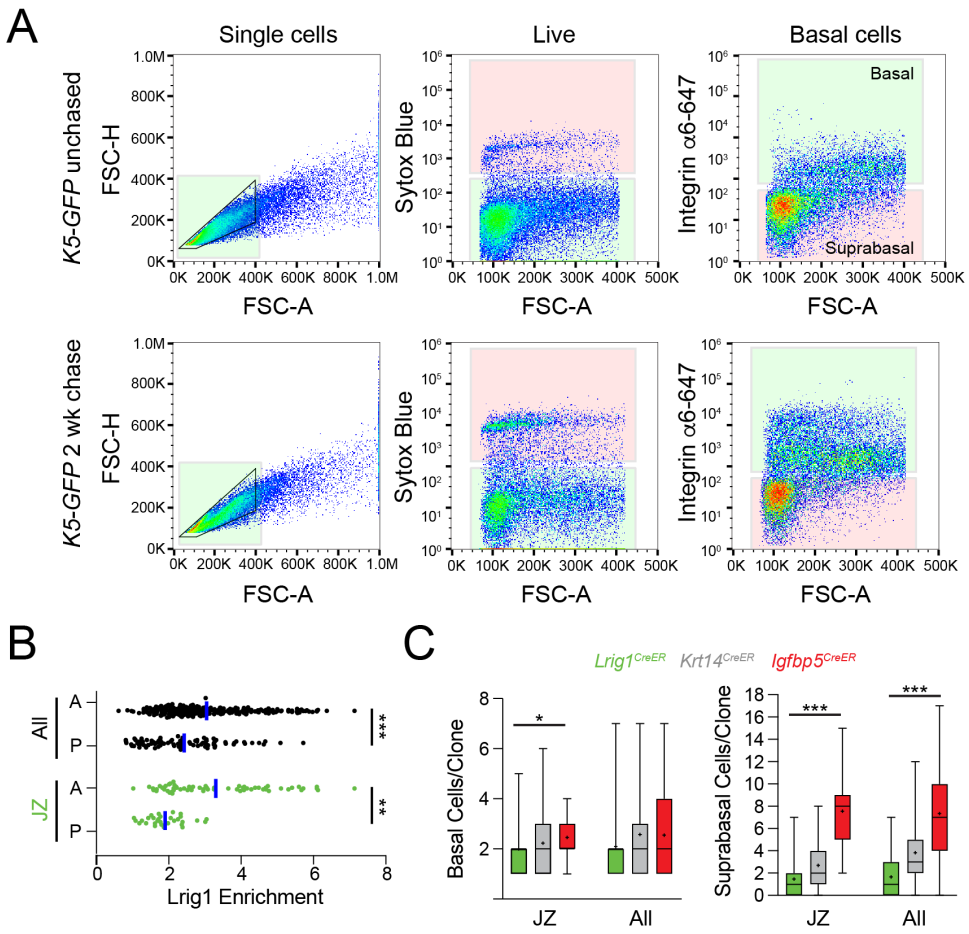

Figure S5, related to Figure 6 | RNAseq reveals Lrig1 is enriched in quiescent OESCs of the JZ.
(A) Sorting strategy for isolating palatal basal cells, related to Fig. 6A. Flow cytometry data for isolated palatal cells from unchased (top, 0 wk dox) and 2 wk chased (bottom) *K5-GFP* mice. Gates are shown for isolating single cells, Sytox blue-live cells, and α6-integrin^{HI} basal cells. (B) Lrig1 enrichment across the whole palate (black) and JZ (green), separated into anterior (A) and posterior (P) regions; mean shown by blue bars. (C) Box and whisker plots of counts of basal cells/clone (left) and suprabasal cells/clone (right) for *Krt14*^{CreER} (gray), *Lrig1*^{CreER} (green) and *Igfbp5*^{CreER} (red) drivers following a 2 wk lineage tracing period. Note trend toward highest numbers of basal and suprabasal cells per clone in *Igfbp5* clones and lowest in *Lrig1* clones. Box and whiskers represent min and max; + = mean. *p<0.05, **p<0.01 ***p<0.0001, by Mann-Whitney test in (B,C).

Figure S6, related to Figure 7

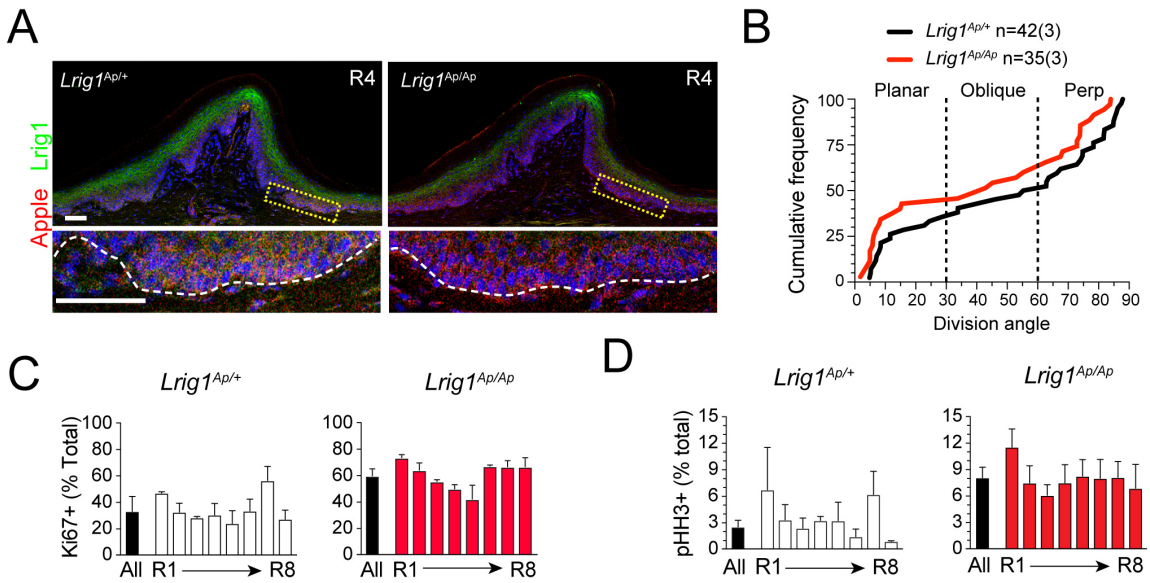

Figure S6, related to Figure 7 | Lrig1 labels JZ LRCs and maintains quiescence.
(A) Lrig1 antibody staining (green) in hard palate in *Lrig1*$^{Ap/+}$ heterozygotes (left) and *Lrig1*$^{Ap/Ap}$ homozygotes (right). The *Lrig1*^{Ap} knockin allele drives Apple fluorescent protein expression (red) from the endogenous promoter, and is a functional null. Yellow boxed areas shown at high magnification below. Lrig1 antibody faithfully colocalizes with *Lrig1*^{Ap} in hets and is lost in nulls, demonstrating antibody specificity. (B) Cumulative frequency plot of division orientation in *Lrig1* heterozygote controls (left, *Lrig1*$^{Ap/+}$) and *Lrig1* knockouts (right, *Lrig1*$^{Ap/Ap}$). Loss of Lrig1 has no obvious impact on OCD patterns. (C,D) Proliferation, as assessed by Ki67 (C) and pHH3 (D), for *Lrig1*$^{Ap/+}$ heterozygotes (left, white bars) and *Lrig1*$^{Ap/Ap}$ knockouts (right, red bars), related to Fig 7K. Loss of Lrig1 in the palate increases cycling (Ki67) and mitosis (pHH3) across the entire palate. Bars in (C,D) represent s.e.m. Scale bar: 50 μm (A).